Observation of defect density dependent elastic modulus of graphene

Hu Li, Emel Gürbüz, Soumyajyoti Haldar, Tanveer Hussain, Xiaoxiao Zheng, Xiaoling Ye, Sylvester Wambua Makumi, Tianbo Duan, Syed Hassan Mujtaba Jafri, Lakshya Daukiya, et al.

▶ **To cite this version:**

Hu Li, Emel Gürbüz, Soumyajyoti Haldar, Tanveer Hussain, Xiaoxiao Zheng, et al.. Observation of defect density dependent elastic modulus of graphene. Applied Physics Letters, 2023, 123 (5), 10.1063/5.0157104 . hal-04195364

HAL Id: hal-04195364
https://hal.science/hal-04195364

Submitted on 4 Sep 2023

HAL is a multi-disciplinary open access archive for the deposit and dissemination of scientific research documents, whether they are published or not. The documents may come from teaching and research institutions in France or abroad, or from public or private research centers.

L'archive ouverte pluridisciplinaire **HAL**, est destinée au dépôt et à la diffusion de documents scientifiques de niveau recherche, publiés ou non, émanant des établissements d'enseignement et de recherche français ou étrangers, des laboratoires publics ou privés.

Observation of defect density dependent elastic modulus of graphene

Hu Li[1,2,3†], Emel Gürbüz[4†], Soumyajyoti Haldar[4,5†], Tanveer Hussain[6], Xiaoxiao Zheng[1,2], Xiaoling Ye[1,2], Sylvester Wambua Makumi[3], Tianbo Duan[3], Syed Hassan Mujtaba Jafri[3,7], Lakshya Daukiya[8], Laurent Simon[8], Amir Karton[6]*, Biplab Sanyal[4]*, and Klaus Leifer[3]*

[1] Shenzhen Research Institute of Shandong University, 518057 Shenzhen, China
[2] Shandong Technology Centre of Nanodevices and Integration, School of Microelectronics, Shandong University, 250101 Jinan, China
[3] Department of Materials Science and Engineering – Ångström Laboratory, Uppsala University, 75121 Uppsala, Sweden
[4] Department of Physics and Astronomy – Ångström Laboratory, Uppsala University, 75121 Uppsala, Sweden
[5] Institute of Theoretical Physics and Astrophysics, University of Kiel, D-24118 Kiel, Germany
[6] School of Science and Technology, University of New England, NSW2351 Armidale, Australia
[7] Department of Electrical Engineering, Mirpur University of Science and Technology, 10250 Mirpur, Azad Jammu and Kashmir, Pakistan
[8] Institut de Sciences des Matériaux de Mulhouse, UMR 7361-CNRS, UHA, France

† These authors contribute equally.

Authors to whom correspondence should be addressed: Klaus Leifer: Klaus.Leifer@angstrom.uu.se; Biplab Sanyal: Biplab.Sanyal@phyics.uu.se; Amir Karton: Amir.Karton@uwa.edu.au

ABSTRACT

The past decade has witnessed a tremendous development of graphene applications in many fields, however, as one of the key considerations, the mechanical properties of graphene still remain largely unexplored. Herein, by employing focused ion beam irradiation, graphene with various defect levels is obtained and further investigated by using Raman spectroscopy, and scanning tunnelling microscopy. Specially, our atomic force microscopy based nanomechanical property measurement demonstrates a clear defect density dependent behaviour in the elastic modulus of graphene on substrate as the defect density is higher than a threshold value of 10^{12} cm^{-2}, where a clear decay is observed in the stiffness of graphene. This defect density dependence is mainly attributed to the appearance of amorphous graphene, which is further confirmed with our molecular dynamics calculations. Therefore, our reported result provides an essential guidance to enable the rational design of graphene materials in nanodevices, especially from the perspective of mechanical properties.

Ever since the isolation, graphene has become one of the topical materials as a versatile platform to study the electronics, magnetics, mechanics and quantum physics phenomena where its simple two-dimensional honeycomb lattice structure is at the origin of a number of anomalous properties [1-8]. As evidenced by a series of experimental and theoretical studies, the physical properties of graphene can be modified by tuning its structures [9-11]. For instance, by engineering the graphene edge with zigzag structure, nonbonding π-electron states can be introduced, which gives graphene spin-polarized electronic properties [12], and similarly, by engineering the graphene edge with armchair structure, size-dependent band gap can be demonstrated [13]. Modification of graphene has great effect on the physical properties of graphene. Except the electronic properties, as the strongest material in nature, the nanomechanical properties of graphene also attracted widespread attention.

Graphene has high elastic modulus (1.02 TPa)[14], and the reason for the extraordinary stiffness of graphene lies in the stability and uniformity of the sp^2 hybridized carbon atoms which form the hexagonal aromatic rings in graphene lattice and oppose a variety of deformations [15, 16]. Exploring the factors which influence the elastic modulus in experimental and computational approaches will have great effect on extending the potential applications of graphene in nanodevices[1, 17-19]. Los et al. [20] obtained explicit expression for the size and strain dependence of graphene's elastic moduli by atomistic simulations, providing an explanation for the anomalous strong variations with strain in recent measurements of the elastic modulus. In addition to the size-dependence of the in-plane elastic moduli, the defects on graphene also influence

graphene's mechanical property. It is commonly assumed that the defect can deteriorate the mechanical properties of graphene due to the breaking of the sp^2 hybridized carbon network, but the real situation is more complicated. For instance, López-Polín et al,. [21] studied the mechanical properties of freestanding graphene and it is found that the elastic modulus of graphene increases when the defect level is extremely low. However, how the defect density influences mechanical properties of graphene in a wide range of defect density still remains as a question, especially for more practical graphene system such as supported graphene (graphene on substrate), which play a crucial role in determining the stability and performance of the nanodevices.

In this work, we have employed the focused ion beam (FIB) irradiation in high vacuum to obtain supported graphene with different defect densities. Our atomic force microscopy (AFM) based elastic modulus measurements find that graphene shows a clear defect density dependent behaviour in the elastic modulus. When the defect density is lower than 10^{12} cm^{-2}, the stiffness of graphene remains nearly unchanged, showing a plateau when plotting the elastic modulus as a function of defect density, but a clear decay will be revealed as the defect level becomes higher.

A Renishaw Raman spectroscope with 532 nm excitation was employed to characterize the structure modifications in graphene. The the effect crystallite size L_a (nm) and defect density $n_D(cm^{-2})$ of graphene under ion irradiation can be calculated as:

$$L_a = C(\lambda)(\frac{I_D}{I_G})^{-1} \quad (1)$$

$$L_a = \sqrt{C'(\lambda)^{-1}(\frac{I_D}{I_G})} \quad (2)$$

$$n_D = 10^{14}/(\pi L_a^2) \quad (3)$$

where $C(\lambda)$ and $C'(\lambda)$ are constants relating to the wavelength of the incoming Raman scattering light. Equation (1) applied in the first phase that the intensity ratio of I_D/I_G (as shown in Figure 1b) increases with the applied ion dosage and the Equation (2) applied in the second phase that the intensity ratio of I_D/I_G decreases with the applied ion dosage.

Peak force quantitative nanomechanical mapping mode in a Bruker Multimode 8 atomic force microscopy (AFM) was utilized in this work to characterize the elastic modulus of the graphene/SiO_2 system as well as bare SiO_2 by using an antimony doped Si tip (300 N/m) with an 8 nm radius [22,23]. To obtain the elastic modulus E, the Derjaguin-Muller-Toporov (DMT) model is employed and can be expressed as [24-26]:

$$F - F_0 = \frac{4}{3}E^*\sqrt{R(d-d_0)^3} \quad (4)$$

$$E^* = [\frac{1-\nu_{tip}^2}{E_{tip}} + \frac{1-\nu_s^2}{E_s}]^{-1} \quad (5)$$

where $F - F_0$ is the force applied on the AFM cantilever relative to zero force, R is the tip radius and $d - d_0$ is the sample deformation.

The calculations for the generation of crystallite graphene and amorphous graphene structures were done by classical molecular dynamics (CMD) with the open source LAMMPS package [27] employing the Tersoff potential [28]. Crystallite graphene flakes were produced by adding 10 Å space along x-y directions in the following supercells; (18x18), (20x20), (23x23), (25x25), (30x30), (35x35), (40x40), (45x45), (50x50) where the lattice parameter of the unit cell was considered as 2.46 Å and the vacuum region was taken to be 40 Å. The generation of amorphous graphene structures were initiated by distributing atoms randomly into the defined 2D crystallite graphene supercells mentioned above. These random initial structures were subjected to the following procedures; heating at 5000 K; fast-quenching to 2000 K with a 51.28×10^{14} K/s cooling rate; applying short equilibration at 2000 K for 135 fs; quenching to 300 K with a 49.71×10^{13} K/s cooling rate and the final equilibrating step at 300 K for 3420 fs. We used Berendsen thermostat [29] for temperature re-scaling with 45 fs relaxation time with 1 fs time step. After obtaining the periodic 2D amorphous structures, the amorphous graphene flakes were prepared by adding 10 Å space along x-y directions. Thereafter, force minimization of the nanocrystallite graphene and amorphous graphene flakes was done at T = 0 K with a stopping energy tolerance of 1×10^{-18} eV. Binding energies BE of the systems were obtained from: $\mathrm{BE} = -[E_{system} - nE_C/n]$, where E_{system} is the system's total energy, E_C is the energy of a single C atom and n is the total number of atoms.

Large-scale monolayer graphene synthesized by chemical vapour deposition (CVD) and transferred to SiO_2/Si substrate [30, 31] was employed. The structural modification of graphene samples was induced by using focused ion beam (30 kV Ga^+) irradiation in a FEI Strata DB235 (FIB/SEM) with ion dosages ranging from 10^{12} to 5×10^{14} ions/cm^2 under a vacuum condition of 10^{-6} mbar [32,33]. As compared with plasma techniques [34, 35], the advantage of employing high energy ions for the modification of graphene is that, after bombarding the carbon atoms, the ions can penetrate into the substrate deeply and do neither substitute carbon atoms nor accumulate on the graphene surface (see supporting information Figure S1). Therefore, there are no sp^3 adatoms (e.g. O binds to graphene in Oxygen plasma) on top of the graphene sheet and the structural modification in graphene will only occur in the created defect or boundary region, which will make the following analysis and especially their interpretation easier.

To quantitatively analyse the structural modifications in graphene, Raman spectroscopy was employed and the evolution of the Raman spectra of graphene samples under ion irradiation is shown in Figure 1a. It can be seen that the D peak (at ~1350 cm^{-1}), the indicative of disorder, rises

considerably and becomes prominent with increased ion dosages, whereas conversely the 2D peak (~2700 cm^{-1}) becomes less intensive and broad. When we plot the intensity ratio I_D/I_G as shown in Figure 1b, we observe a considerable increase of this ratio with increasing ion doses and a maximum intensity ratio I_D/I_G of 3.4 at an ion dose of 10^{13} ions/cm^2, where after the ratio decreases clearly and reaches about 0.7 for the highest ion dose [36, 37]. This inverted V-curve phenomenon in the I_D/I_G plot of graphene is commonly explained as a transition where the first stage (I_D/I_G increases with ion dosage) indicates the transition from graphene to nanocrystalline graphene and the second stage (I_D/I_G increases with ion dosage) indicates the transition from nanocrystalline graphene to amorphous graphene. To better illustrate the defect level in graphene under ion irritation, the defect density as a function of the ion dosage is plotted in Figure 1c, from which it can be seen that the defect density monotonically increases with the dosages, which indicates a clear tendency that more ion irradiation leads to higher defect levels in graphene, which agrees well with previous reported [38, 39].

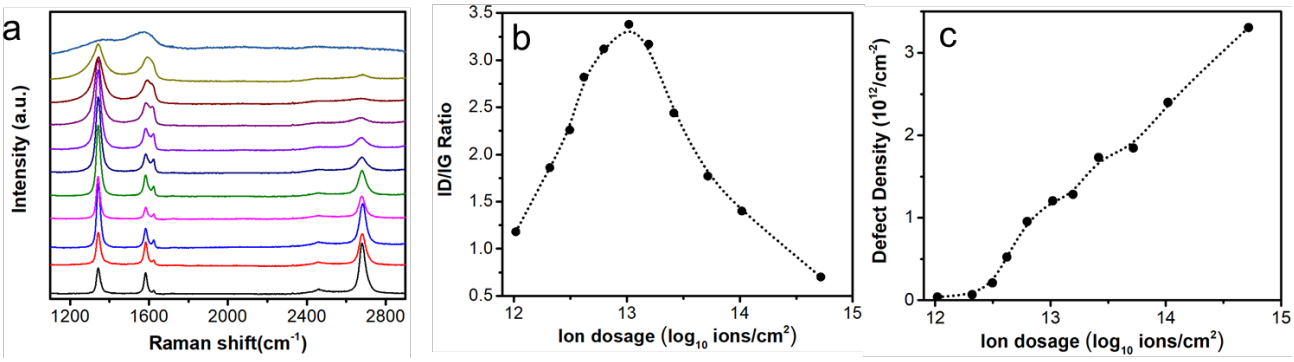

Figure 1. Raman analysis of the structure modifications in graphene under ion irradiation. (a) Evolution of graphene on top of SiO_2 substrate under the ion dosages from bottom to up: 10^{12}, 2×10^{12}, 3×10^{12}, 4×10^{12}, 6×10^{12}, 10^{13}, 2×10^{13}, 3×10^{13}, 5×10^{13}, 10^{14}, 5×10^{14} ions/cm^2. (b) Raman peak intensity ratios of I_D/I_G as a function of applied ion dosages. (c) Defect density as a function of applied ion dosages.

To better understand the structure modification, scanning tunnelling microscopy (STM) was employed to characterize the structure of graphene by obtaining atomic resolution STM images as shown in Figure 2. Figure 2a depicts the STM image of graphene at lowest ion dosage irradiation with a defect density of 4×10^{10} cm^{-2}, and it can be seen that the main area remains a close to perfect graphene crystal. After having exposed the sample to highest ion dose irradiation (a defect density of 3.3×10^{12} cm^{-2}), we observe the graphene areas with strongly reduced crystallite lattice contrast. From previous Raman studies on the defected graphene, the sample in Figure 2b with a very low intensity ratio I_D/I_G of 0.7 is normally considered as amorphous graphene.

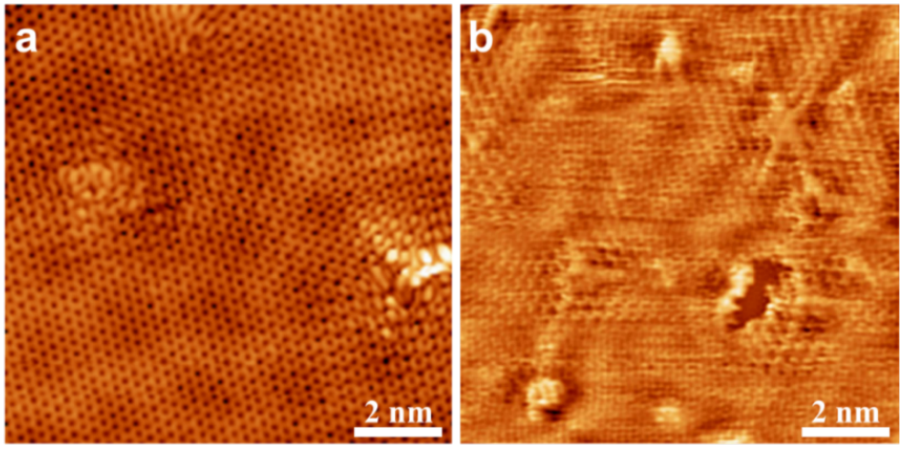

Figure 2. STM images of graphene. Under the ion dosages of (a) 10^{12} ions/cm^2 and (b) 5×10^{14} ions/cm^2, respectively.

Prior to the elasticity characterization of the graphene on SiO_2 system, we have performed the AFM based nanoindentation of the bare SiO_2 substrate under the same ion irradiation conditions. From the AFM height image (Figure 3a), it can be seen clearly that there is a height contrast between the ion irradiated area and non-irradiated area due to the ion implantation [40], leading to the slight increase in the height of the ion irradiated area, also known as swelling effect. However, the reconstructed elasticity mapping shows a uniform contrast in the image between the two areas (Figure 3b), which indicates that there is no stiffness difference. Therefore, the ion irradiation does not modify the elastic modulus of the SiO_2 as shown in Figure 3c.

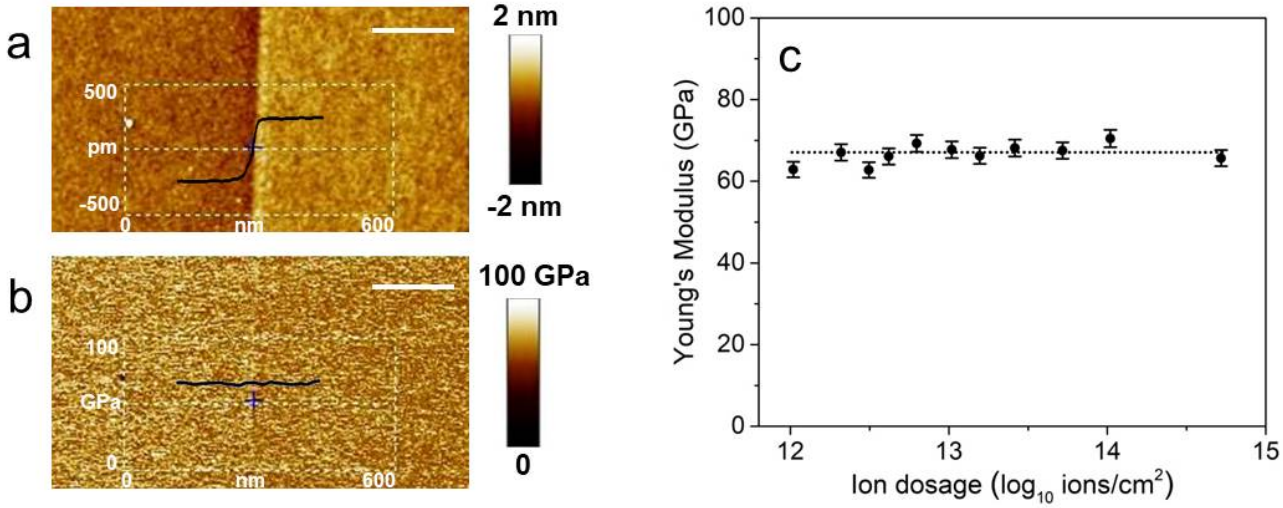

Figure 3. Substrate analysis under ion irradiation. (a) Height and (b) reconstructed elastic modulus mapping of the SiO_2 under 5×10^{14} ions/cm^2 ion irradiation. The inserted graphs show the profiles crossing the irritated and non-irradiated areas. The scale bar is 200 nm (c) Plotted Young's modulus of the SiO_2 as a function of applied ion dosages. The irradiation condition on SiO_2 is as the same as the graphene on SiO_2.

In order to understand the evolution of elastic modulus in the system of graphene on SiO_2, a series of samples was prepared and then characterized by using AFM based nanoindentation [41-43]. Figure 4 displays the recorded force-distance curves of the graphene at low and high defect levels as well as detailed schematic illustration of different phases from the approach and retract process of the AFM nanoindentation. It can be seen clearly that the slopes at the phase II/III are quite different for graphene with different defect density, which indicates that the elastic moduli are distinct. The systematic result on the evolution of the elastic modulus of graphene with various defect density is demonstrated in Figure 5a. Remarkably, it is found that the elastic modulus plot of graphene on SiO_2 can be classified into two regions where a threshold point can be obtained at a defect density of 10^{12} cm^{-2}. When the defect level is lower than 10^{12} cm^{-2}, the elastic modulus remains nearly constant, resulting in a plateau region in the plot. While at a defect density higher than 10^{12} cm^{-2}, the elastic modulus starts to show a considerable drop as the defect density increases. The white dotted line in the plot indicates the elastic modulus of the SiO_2 substrate, and for the graphene with the highest defect density, the Young's modulus decreases below the one of the SiO_2. When taking into account the stagnancy of the elasticity modulus of SiO_2 at increased ion dose in Figure 3b, it can be concluded that the significant drop in the elastic modulus of the graphene on SiO_2 system is mainly attributed to the considerable decrease of the elastic modulus in the graphene. Moreover, it can be found that for graphene sheet on top of SiO_2 with the highest defect density, the elastic modulus is smaller than the one of SiO_2, and therefore the graphene must be softer than SiO_2.

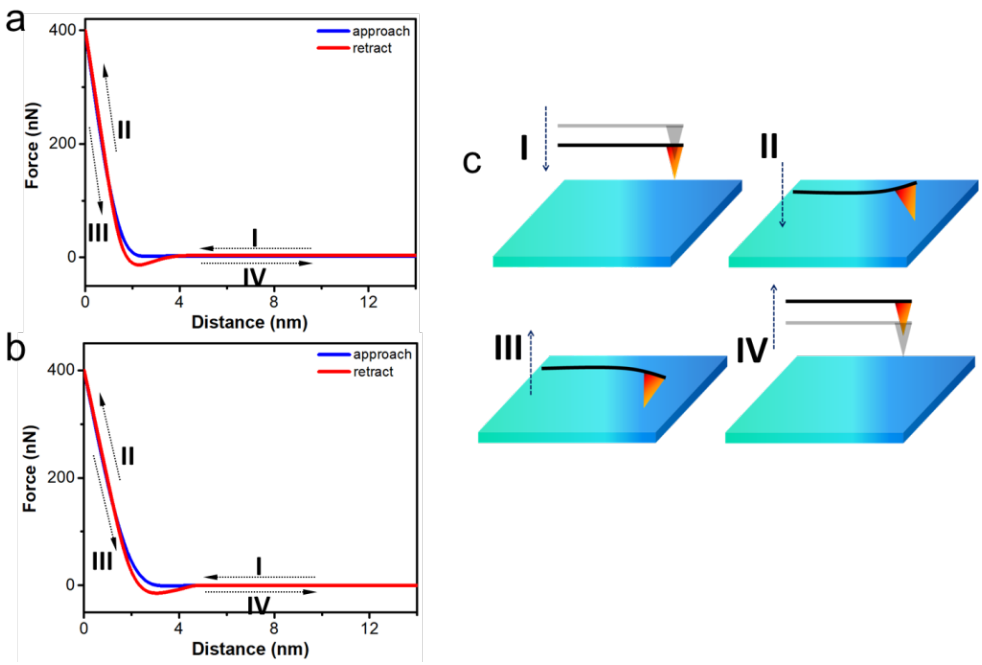

Figure 4. AFM based nanoindentation for nanomechanical measurements. (a) Force-distance curves for graphene with defect density of (a) 4×10^{10} cm^{-2} and (b) 3.3×10^{12} cm^{-2}, (c) schematics of the nanoindentation process for different phases.

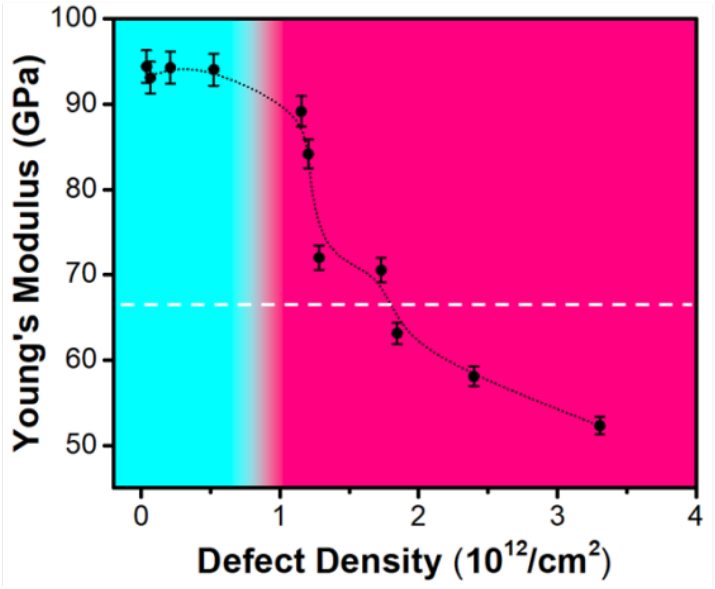

Figure 5. Evolution of the elastic modulus of the graphene on SiO_2 substrate with different defect densities. The white dotted line indicates the elastic modulus of the SiO_2 substrate.

From above Raman and mechanical property characterizations, it is found that the elastic modulus of graphene remains nearly constant within the transition from graphene to nanocrystalline graphene as the defect density lower than 10^{12} cm^{-2}, while a clear decay can be observed within the transition from nanocrystalline graphene to amorphous graphene as the defect density higher than 10^{12} cm^{-2}. Therefore, it can be explained that the decrease in the elastic modulus is mainly attributed to the appearance of the amorphous graphene, which starts to present when the defect density is higher than 10^{12} cm^{-2}. Theoretical calculations have reported a linear correlation between the binding energy and

the elastic modulus of graphene, indicating an approach to invesitigate the mechanical properties of graphene qualitatively by employing theorical methods. To further comfirm the effect of the amorphous graphene on the elastic modulus of graphene, a series of molecular dynamics simulations have been carried out, in which nanocrystalline graphene and amorphous graphene with different sizes were calculated. The obtained binding energy plots are shown in Figure 6. From which it is clear to be seen that the binding energy for amorphous graphene is considerably lower than that of nanocrystalline graphene, which agrees well with our explanations on the deteriorate effect of the amorphousness on the mechanical properties of graphene.

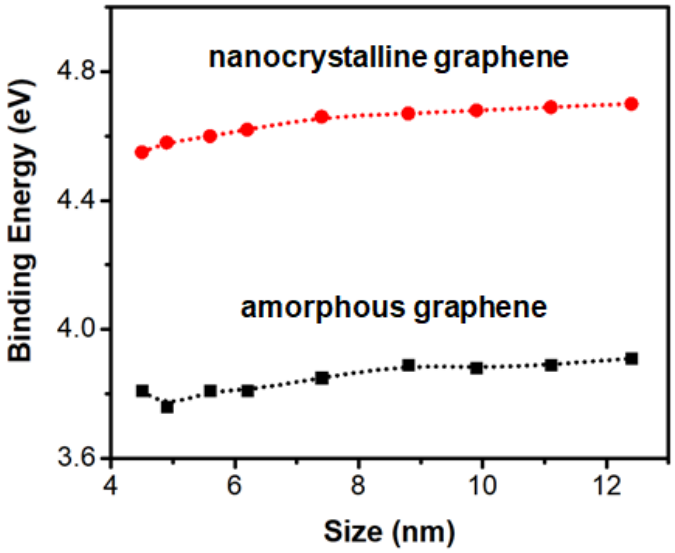

Figure 6. Molecular dynamics calculations of the binding energy with different sizes.

In conclusion, by employing ion irradiation and AFM based nanoindentation techniques, defect density dependent elastic modulus behaviour of graphene is revealed when the defect density is higher than 10^{12} cm^{-2}. It is found from our experiment that, when the defect density is lower than 10^{12} cm^{-2}, the elastic modulus of graphene remains nearly constant, leading to a plateau region when plotting the elastic modulus as a function of defect level. While at a defect density higher than 10^{12} cm^{-2}, the elastic modulus starts to show a considerable decrease as the defect decreases. These results provide an essential guidance to enable the rational design of graphene materials in nanodevices, especially from the perspective of mechanical properties.

See the supplementary material for the XPS analysis of the graphene after ion irradiation of 5×10^{14} ions/cm^2; amorphous and nanocrystalline graphene for molecular dynamics calculations.

The authors are grateful for the financial support from the Swedish Research Council (Grant No.: 2016-05259 and 2016-05366), Swedish Research Links programme (Grant No.: 2017-05447), Shandong Provincial Natural Science Foundation (Grant No.: ZR2022ZD05 and ZR2021QE148), Shandong Provincial Natural Science Foundation for Excellent Young Scientists Fund Program (Overseas) (Grant No.: 2022HWYQ-060), Guangdong Basic and Applied Basic Research Foundation (Grant No.: 2022A1515011473), Olle Engkvist (Grant No.: 211-0068) and Formas (Grant No.: 2019-01538). We also acknowledge the supercomputing time allocation by the Swedish National Infrastructure for Computing (SNIC) and PRACE-2IP project 'CHARTERED2' resource Salomon cluster based in Czech Republic at the IT4Innovations for performing the computations.

AUTHOR DECLARATIONS

Conflict of Interest

The authors have no conflicts to disclose.

Author Contributions

Hu Li: Conceptualization (equal), data curation (equal), writing-original draft preparation (equal), funding acquisition (lead). **Emel Gürbüz:** Conceptualization (equal), formal analysis (equal), writing-original draft preparation (equal). **Soumyajyoti Haldar:** Data curation (equal), formal analysis (equal). **Tanveer Hussain:** Formal analysis (equal), methodology (equal). **Xiaoxiao Zheng:** Formal analysis (equal), writing-review & editing (equal). **Xiaoling Ye:** Methodology (equal), writing-review & editing (equal).

Sylvester Wambua Makumi: Visualization (equal). **Tianbo Duan:** Data curation (equal), writing-original draft preparation (equal). **Syed Hassan Mujtaba Jafri:** Methodology (equal), supervision (equal). **Lakshya Daukiya:** Software (equal), validation (equal). **Laurent Simon:** Software (equal), validation (equal). **Amir Karto:** Software (equal), validation (equal). **Biplab Sanyal:** Software (equal), validation (equal), writing-original draft preparation (equal). **Klaus Leifer:** Conceptualization (equal), writing-review & editing (equal).

DATA AVAILABILITY

The data that support the findings of this study are available within the article [and its supplementary material].

REFERENCES

(1) Geim, A. K., NOVOSELOV, K. S., "The rise of graphene," Nat. Mater. **6**, 183–191 (2007).
(2) Allen, M. J., Tung, V. C., Kaner, R. B., "Honeycomb Carbon: A Review of Graphene," Chem. Rev. **110**, 132–145 (2010).
(3) Novoselov, K. S., Fal'ko, V. I., Colombo, L., Gellert, P. R., Schwab, M. G., Kim, K., "A roadmap for graphene," Nature **490** (7419), 192-200 (2012).
(4) Hollen, S. M., Gupta, J. A., "Painting magnetism on a canvas of graphene," Science **352**, 415–416 (2016).
(5) Tucek, J., Blonski, P., Ugolotti, J., Swain, A. K., Enoki, T., Zboril, R., "Emerging chemical strategies for imprinting magnetism in graphene and related 2D materials for spintronic and biomedical applications," Chem Soc Rev **47** (11), 3899-3990 (2018).
(6) Castro Neto, A. H., Guinea, F., Peres, N. M. R., Novoselov, K. S., Geim, A. K., "The electronic properties of graphene," Reviews of Modern Physics **81** (1), 109-162 (2009).
(7) Li, H., Papadakis, R., Hussain, T., Karton, A., Liu, J., "Moiré patterns arising from bilayer graphone/graphene superlattice," Nano Research **13** (4), 1060-1064 (2020).
(8) Sevik, C., "Assessment on lattice thermal properties of two-dimensional honeycomb structures: Graphene,h-BN,h-MoS2, andh-MoSe2," Physical Review B **89** (3), (2014).
(9) Son, Y. W., Cohen, M. L., Louie, S. G., "Half-metallic graphene nanoribbons," Nature **444** (7117), 347-9 (2006).
(10) Hod, O., Barone, V. n., Peralta, J. E., Scuseria, G. E., "Enhanced half-metallicity in edge-oxidized zigzag graphene nanoribbons," Nano Lett. **7** 2295–2299 (2007).
(11) Stampfer, C., Guttinger, J., Hellmuller, S., Molitor, F., Ensslin, K., Ihn, T., "Energy gaps in etched graphene nanoribbons," Phys Rev Lett **102** (5), 056403 (2009).
(12) Su, X., Xue, Z., Li, G., Yu, P., "Edge State Engineering of Graphene Nanoribbons," Nano Lett **18** (9), 5744-5751 (2018).
(13) Merino-Diez, N., Garcia-Lekue, A., Carbonell-Sanroma, E., Li, J., Corso, M., Colazzo, L., Sedona, F., Sanchez-Portal, D., Pascual, J. I., de Oteyza, D. G., "Width-Dependent Band Gap in Armchair Graphene Nanoribbons Reveals Fermi Level Pinning on Au(111)," ACS Nano **11** (11), 11661-11668 (2017).
(14) Cao, G., "Atomistic Studies of Mechanical Properties of Graphene," Polymers **6** (9), 2404-2432 (2014).
(15) Papageorgiou, D. G., Kinloch, I. A., Young, R. J., "Mechanical properties of graphene and graphene-based nanocomposites," Progress in Materials Science **90**, 75-127 (2017).
(16) Booth, T. J., Blake, P., Nair, R. R., Jiang, D., Hill, E. W., Bangert, U., Bleloch, A., Gass, M., Novoselov, K. S., Katsnelson, M. I., Geim, A. K., "Macroscopic graphene membranes and their extraordinary stiffness," Nano Lett. **8** (8), 2442–2446 (2008).
(17) Lee, C., Wei, X., Kysar, J. W., Hone, J., "Measurement of the Elastic Properties and Intrinsic Strength of Monolayer Graphene," Science **321**, 385–388 (2008).
(18) Košmrlj, A., Nelson, D. R., "Response of thermalized ribbons to pulling and bending," Physical Review B **93** (12), (2016).
(19) Los, J. H., Fasolino, A., Katsnelson, M. I., "Mechanics of thermally fluctuating membranes," npj 2D Materials and Applications **1** (1), (2017).
(20) Los, J. H., Fasolino, A., Katsnelson, M. I., "Scaling Behavior and Strain Dependence of In-Plane Elastic Properties of Graphene," Phys Rev Lett **116** (1), 015901 (2016).
(21) López-Polín, G., Gómez-Navarro, C., Parente, V., Guinea, F., Katsnelson, Mikhail I., Pérez-Murano, F., Gómez-Herrero, J., "Increasing the elastic modulus of graphene by controlled defect creation," Nature Physics **11** (1), 26-31 (2014).
(22) Bhattacharya, K., El-Sayed, R., Andón, F. T., Mukherjee, S. P., Gregory, J., Li, H., Zhao, Y., Seo, W., Fornara, A., Brandner, B., Toprak, M. S., Leifer, K., Star, A., Fadeel, B., "Lactoperoxidase-mediated degradation of single-walled carbon nanotubes in the presence of pulmonary surfactant," Carbon **91**, 506-517 (2015).
(23) El-Sayed, R., Bhattacharya, K., Gu, Z., Yang, Z., Weber, J. K., Li, H., Leifer, K., Zhao, Y., Toprak, M. S., Zhou, R., Fadeel, B., "Single-Walled Carbon Nanotubes Inhibit the Cytochrome P450 Enzyme, CYP3A4," Sci Rep **6**, 21316 (2016).
(24) DERJAGUIN, B. V., MULLER, V. M., TOPOROV, Y. P., "Effect of contact deformations on the adhesion of particles," J. Colloid Interface Sci **53**, 314–326 (1975).
(25) Drelich, J., Tormoen, G. W., Beach, E. R., "Determination of solid surface tension from particle-substrate pull-off forces measured with the atomic force microscope," J Colloid Interface Sci **280** (2), 484-97 (2004).
(26) Cai, Y., Li, H., Karlsson, M., Leifer, K., Engqvist, H., Xia, W., "Biomineralization on single crystalline rutile: the modulated growth of hydroxyapatite by fibronectin in a simulated body fluid," RSC Advances **6** (42), 35507-35516 (2016).

(27) Plimpton, S., "Fast Parallel Algorithms for Short-Range Molecular Dynamics," J. Comput. Phys. **117** 1–19 (1995).
(28) Tersoff, J., "Chemical order in amorphous silicon carbide," Phys Rev B Condens Matter **49** (23), 16349-16352 (1994).
(29) Berendsen, H. J. C., Postma, J. P. M., van Gunsteren, W. F., DiNola, A., Haak, J. R., "Molecular dynamics with coupling to an external bath," The Journal of Chemical Physics **81** (8), 3684-3690 (1984).
(30) Li, X., Cai, W., An, J., Kim, S., Nah, J., Yang, D., Piner, R., Velamakanni, A., Jung, I., Tutuc, E., Banerjee, S. K., Colombo, L., Ruoff, R. S., "Large-area synthesis of high-quality and uniform graphene films on copper foils," Science **324**, 1312–4 (2009).
(31) Liang, X., Sperling, B. A., Calizo, I., Cheng, G., Hacker, C. A., Zhang, Q., Obeng, Y., Yan, K., Peng, H., Li, Q., Zhu, X., Yuan, H., Walker, A. R. H., Liu, Z., Peng, L.-m., Richter, C. A., "Toward clean and crackless transfer of graphene," ACS Nano **5**, 9144–53 (2011).
(32) Jafri, S. H. M., Carva, K., Widenkvist, E., Blom, T., Sanyal, B., Fransson, J., Eriksson, O., Jansson, U., Grennberg, H., Karis, O., Quinlan, R. A., Holloway, B. C., Leifer, K., "Conductivity engineering of graphene by defect formation," Journal of Physics D: Applied Physics **43** (4), (2010).
(33) Li, H., Wani, I. H., Hayat, A., Jafri, S. H. M., Leifer, K., "Fabrication of reproducible sub-5 nm nanogaps by a focused ion beam and observation of Fowler-Nordheim tunneling," Applied Physics Letters **107** (10), (2015).
(34) Wu, J., Xie, L., Li, Y., Wang, H., Ouyang, Y., Guo, J., Dai, H., "Controlled chlorine plasma reaction for noninvasive graphene doping," J Am Chem Soc **133** (49), 19668-71 (2011).
(35) Zandiatashbar, A., Lee, G. H., An, S. J., Lee, S., Mathew, N., Terrones, M., Hayashi, T., Picu, C. R., Hone, J., Koratkar, N., "Effect of defects on the intrinsic strength and stiffness of graphene," Nat Commun **5**, 3186 (2014).
(36) Ferrari, A. C., "Raman spectroscopy of graphene and graphite: Disorder, electron–phonon coupling, doping and nonadiabatic effects," Solid State Communications **143** (1-2), 47-57 (2007).
(37) Lucchese, M. M., Stavale, F., Ferreira, E. H. M., Vilani, C., Moutinho, M. V. O., Capaz, R. B., Achete, C. A., Jorio, A., "Quantifying ion-induced defects and Raman relaxation length in graphene," Carbon **48** (5), 1592-1597 (2010).
(38) Wang, Q., Mao, W., Ge, D., Zhang, Y., Shao, Y., Ren, N., "Effects of Ga ion-beam irradiation on monolayer graphene," Applied Physics Letters **103** (7), (2013).
(39) Li, H., Daukiya, L., Haldar, S., Lindblad, A., Sanyal, B., Eriksson, O., Aubel, D., Hajjar-Garreau, S., Simon, L., Leifer, K., "Site-selective local fluorination of graphene induced by focused ion beam irradiation," Sci Rep **6**, 19719 (2016).
(40) Archanjo, B. S., Barboza, A. P., Neves, B. R., Malard, L. M., Ferreira, E. H., Brant, J. C., Alves, E. S., Plentz, F., Carozo, V., Fragneaud, B., Maciel, I. O., Almeida, C. M., Jorio, A., Achete, C. A., "The use of a Ga+ focused ion beam to modify graphene for device applications," Nanotechnology **23** (25), 255305 (2012).
(41) Sun, F., Li, H., Leifer, K., Gamstedt, E. K., "Rate effects on localized shear deformation during nanosectioning of an amorphous thermoplastic polymer," International Journal of Solids and Structures **129**, 40-48 (2017).
(42) Liu, J., Papadakis, R., Li, H., "Experimental observation of size-dependent behavior in surface energy of gold nanoparticles through atomic force microscope," Applied Physics Letters **113** (8), (2018).
(43) Li, H., Han, Y., Duan, T., Leifer, K., "Size-dependent elasticity of gold nanoparticle measured by atomic force microscope based nanoindentation," Applied Physics Letters **115** (5), (2019).